Advanced Mechanical and Mechatronic Systems

Research Article
Volume 2(2), 2026, 122−133
https://doi.org/10.53623/amms.v2i2.1134

Magnetic and Structural Properties of $(Nd_{1-x}Ce_x)Fe_{11}Ti$ Alloys After Melt-Spinning and Nitriding

Jamal Shehu[1,2]*, Igor V. Shchtenin[1], Alexy O. Rodin[1], Zubaida Gali Habib[2]

[1]National Research Technological University (MISIS), Leninsky Prospekt 4, 119049, Moscow, Russia
[2]Yusuf Maitama Sule Federal University of Education Kano, P.M.B 3045 Kano, Nigeria

*Corresponding author: m1707549@edu.misis.ru

SUBMITTED: 25 March 2026; REVISED: 12 June 2026; ACCEPTED: 16 June 2026

ABSTRACT: This study investigates the effect of cerium doping (x = 0 – 0.3) on the structure and magnetic properties of $(Nd_{1-x}Ce_x)Fe_{11}Ti$ alloys processed by melt-spinning and subsequent high-pressure nitriding. X-ray fluorescence confirms compositions close to the intended stoichiometry (impurities <1 wt%). X-ray diffraction reveals a predominant $ThMn_{12}$-type $NdFe_{11}TiN$ phase, with minor α-Fe, and nitriding increases unit cell volume by 5–7%, confirming interstitial nitrogen incorporation. Magnetic hysteresis measurements show substantial enhancement in coercivity and remanence compared to as-cast and melt-spun states. The maximum coercivity (112.9 kA/m) is achieved at x = 0.3, while the highest saturation magnetization (137.0 A·m²/kg) occurs at x = 0.2. These results demonstrate that partial substitution of Nd with more abundant and lower-cost Ce, combined with nitriding, offers a viable pathway toward cos-effective permanent magnets with competitive performance.

KEYWORDS: Melt-spinning; nitriding; intermetallic compounds; coercive force, permanent magnet; residual magnetization

1. Introduction

Rare-earth-transition metal intermetallics with $ThMn_{12}$-type structure (a tetragonal lattice, space group I4/mmm) are promising high-performance permanent magnets because high saturation magnetization, large magnetocrystalline anisotropy the tendency of magnetic moments to align along a specific crystallographic direction, critical for permanent magnet coercivity (strong directional preference of magnetic moments) and good thermal stability [1, 2]. Among these, $NdFe_{11}Ti$-based compounds serve as potential alternatives to $Nd_2Fe_{14}B$, especially interstitial introduction of nitrogen atoms into the lattice [3, 4]. This combination makes the alloy family valuable for both fundamental magnetic studies and practical magnetic development [5, 6]. $NdFe_{11}Ti$-based compounds crystallizes in the tetragonal $ThMn_{12}$ structure (space group I4/mmm – a body-centered tetragonal lattice with a characteristic arrangement of transition metal atoms). Ti atoms preferentially occupy Fe sublattices, particularly the 8i sites, disrupting Fe–Fe "dumbbell" environments that destabilize the parent $NdFe_{12}$ phase. This substitution stabilizes the single 1:12 phase, typically formed within 800–1200 °C, although it slightly reduces the saturation magnetization due to dilution of the Fe sublattice [7, 8]. Processing routes such as arc melting with annealing, melt-spinning, and mechanical alloying

have been employed to obtain high fractions of the 1:12 phase. Secondary phases like α-Fe or Nd_2Fe_{17} must be suppressed, as they significantly deteriorate coercivity [9–11].

The interstitial elements occupy the 2b site of the $ThMn_{12}$ lattice and strong influence on electronic and magnetic properties. First-principles studies have shown that nitrogen is the most effective dopant among B, C, N, O, and F, as it enhances both magnetization and uniaxial anisotropy by strengthening Nd–Fe crystal-field interactions [12, 13]. Experimental results confirm that nitrogenation substantially raise both T_C and anisotropy, producing the technologically important $NdFe_{11}TiN_x$ phase [14]. $NdFe_{11}Ti$ exhibits uniaxial anisotropy at room temperature, driven mainly by Nd-4f crystal fields. Nitrogenation strengthens this effect (i.e. increases the energy barrier for rotating the magnetization away from the easy axis), and anisotropy fields up to ~8 T at room temperature have been reported for $NdFe_{11}TiN_x$ [15]. Ti substitution reduces saturation magnetization compared to hypothetical $NdFe_{12}$, but nitrogenation compensates by enhancing Fe–N hybridization and band filling effects. Studies consistently find higher $\mu_0 M_s$ in $NdFe_{11}TiN_x$ compared to its non-nitrogenated counterpart [16]. Coercivity in $NdFe_{11}Ti$-based alloys is strongly influenced by grain size, phase fraction, and secondary-phase distribution. Rapid solidification followed by annealing yields fine 1:12 grains with improved coercivity, while nitrogenation further increases anisotropy and H_k [9, 11]. Mechanical alloying followed by nitriding can also produce nanostructured materials with enhanced domain wall pinning [11].

Partial substitution of Nd with other rare-earth elements such as Ce, Dy, or La modifies anisotropy and thermal stability. Ce, for example, reduces anisotropy at low temperatures due to its 4f-electron configuration, [17] Ce typically exhibits a mixed or tetravalent state, leading to weaker crystal-field interactions compared to Nd. In recent years, large gap for $ThMn_{12}$-type magnets has been observed due to an excellent combination of intrinsic properties by the prescribed magnetic alloys [18]. On the transition-metal sublattice, Co addition can partially offset Ti's negative effect on magnetization while retaining phase stability. Other stabilizers such as Mo and V have also been used to improve nitridation and high-temperature performance [6, 19]. Moreover, $NdFe_{11}Ti$ remains the canonical bulk-stabilized $ThMn_{12}$ compound. Its nitrogenated derivative $NdFe_{11}TiN_x$ combines high T_c (~700 K), strong anisotropy, and competitive saturation magnetization, rivaling $Nd_2Fe_{14}B$ in intrinsic performance [11]. Future development will depend on refining processing methods to suppress secondary phases, optimize interstitial content, and explore Co-substitution strategies to balance phase stability with magnetic performance [15]. Nitriding of $ThMn_{12}$-type compounds results in lattice expansion, increase in unit cell volume, typically 3 – 7% due to nitrogen occupying interstitial 2b sites and enhanced magnetic anisotropy, which significantly improves coercivity [19]. Substitution of Nd with Ce, an abundant and less expensive rare-earth element, has been explored to reduce costs and partially mitigate the supply risk associated with Nd [20]. However, the effect of Ce substitution on nitrided $NdFe_{11}Ti$ alloys remains insufficiently studied. This research focuses on synthesizing $(Nd_{1-x}Ce_x)Fe_{11}Ti$ alloys (x = 0 – 0.3), processing them by melt-spinning, and subsequently nitriding under high-pressure nitrogen gas. The relationship between structural evolution and magnetic hysteresis properties is systematically evaluated.

2. Experimental methods

2.1. Alloy preparation.

Alloys of nominal composition $(Nd_{1-x}Ce_x)Fe_{11}Ti$ (x = 0, 0.1, 0.2, 0.3) were prepared by arc – melting under an argon atmosphere from high-purity constituent elements (Nd, Ce, Fe, Ti, and minor additions). The melts were re-melting three times to ensure compositional homogeneity.

2.2. Melt-spinning process.

The molten alloys were rapidly solidified via melt-spinning at a wheel speed of 30 m/s to produce thin ribbons. The melt-spinning was performed using a single-roller copper wheel (250 mm diameter) rotating at a tangential speed of 30 m/s. the molten alloy was ejected through a 0.8 mm quartz nozzle under an argon overpressure of 0.2 atm. The nozzle-to-wheel distance was maintained at 2 mm, giving an estimated cooling rate of $\approx 10^6$ K/s. The resulting ribbons were 30-50 μm thick and 1-3 mm wide. This rapid solidification technique aimed to refine the microstructure and enhance the homogeneity of the magnetic phase distribution.

2.3. Nitriding treatment.

The ribbons were nitrided in a high-pressure furnace at 40 atm N_2 and 430 °C for 40 hours. The ribbons (≈2 g per batch) were placed in a quartz boat, and the furnace was evacuated to $<10^{-2}$ mbar before introducing nitrogen gas (99.999% purity). Pressure was maintained within ±0.5 atm using an automatic controller. The temperature was ramped at 10 ℃/min to 430 ℃ and held for 40 hours (±0.5 ℃ stability). No significant deviations in pressure or temperature were observed beyond these tolerances. After nitriding, the furnace was cooled to room temperature under 40 atm N_2 at an uncontrolled rate (≈5 ℃/min). The nitriding step aimed to introduce nitrogen into interstitial sites, increasing lattice parameters and magnetic anisotropy.

2.4. Characterization.

Elemental compositions were determined using X-ray fluorescence (XRF). Structural analysis was conducted by X-ray diffraction (XRD) using Co-Kα radiation. Magnetic hysteresis loops were measured with vibrating sample magnetometer (VSM) at room temperature in a field of 20 kOe to determine coercive force (iHc), residual magnetization (σr), and saturation magnetization (σs).

3. Results

3.1. Elemental composition.

XRF confirmed that the alloys closely matched the intended stoichiometry, with Nd and Ce contents varying according to the substitution level (Table 1). Impurity content was below 1 wt% in all cases, ensuring minimal interference with magnetic behavior [17, 18].

Table 1. X-ray fluorescence spectral analysis result corresponding to the intermetallic compound $(Nd_{1-x}Ce_x)Fe_{11}Ti$.

Alloys (*values of x-parameter*)	**Elemental Content (*mass %*)**				***Impurities***
	Nd	Ce	Fe	Ti	Hf, Mo, Nb, Zr, Cu, Ni, Co, Cr, Si, Al
0	17.89	0	76.18	5.94	≤ 0.5
	17.9 ± 0.07	0	75.4 ± 0.08	6.2 ± 0.05	
0.1	16.11	1.74	76.18	5.94	≤ 0.8
	16.9 ± 0.04	2.1 ± 0.04	74.1 ± 0.03	6.1 ± 0.02	
0.2	14.32	3.48	76.26	5.94	≤ 0.8
	15.9 ± 0.04	3.7 ± 0.04	73.7 ± 0.02	5.9 ± 0.02	
0.3	12.54	5.22	76.30	5.94	≤ 0.7
	13.7 ± 0.04	5.6 ± 0.05	73.8 ± 0.03	6.2 ± 0.02	

3.2. Structural analysis.

Tables 2–5 show XRD results after nitriding and schematically represented in Figure 1. The major phase in all alloys was $NdFe_{11}TiN$ with the $ThMn_{12}$-type tetragonal structure (space group I4/mmm). A secondary α-Fe phase was also detected, with its volume fraction increasing to 30–35% for x = 0.1–0.2. The unit cell volume of $NdFe_{11}TiN$ increased with Ce substitution and nitriding, from 361.60 Å³ for x = 0 to 376.00 Å³ for x = 0.3, reflecting nitrogen incorporation.

Table 2. Results of *X*-ray analysis of the $NdFe_{11}TiN$ alloy after melt spinning (speed = 30 m/s) and subsequent nitriding at a pressure of gaseous medium of about 40 atm and temperature of 430 °C for 40 hours.

Phase composition (Spatial group)	**Volume, %**	**Crystal lattice parameters**			**Unit cell volume *V*, Å³**
		a, Å *b*, Å	*c*, Å	*c/a*	
$NdFe_{11}TiN$ (139 : *I4/mmm*)	90.0(3)	8.645(4) 8.645(4)	4.838(3)	0.560	361.60(14)
α-Fe (229 : *Im-3m*)	10.0(8)	2.870(3) 2.870(3)	2.870(3)	1	23.64(15)

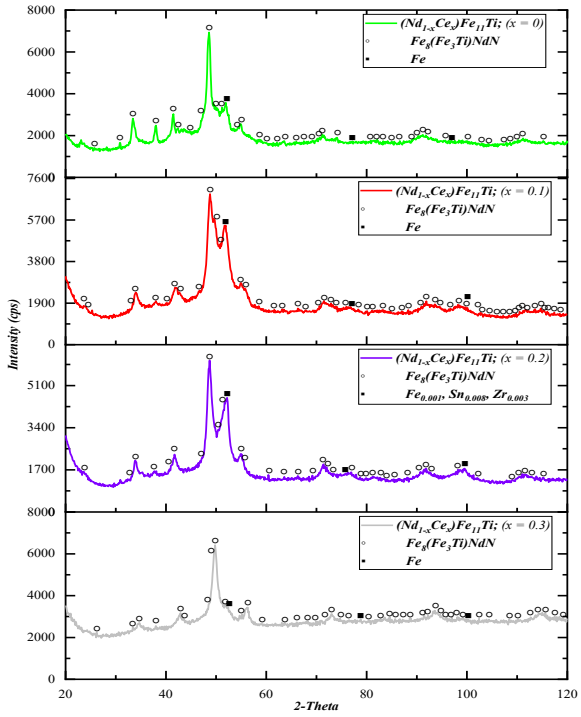

Figure 1. *X*RD pattern of $NdFe_{11}Ti$, $(Nd_{0.9}Ce_{0.1})Fe_{11}Ti$, $(Nd_{0.8}Ce_{0.2})Fe_{11}Ti$, $(Nd_{0.7}Ce_{0.3})Fe_{11}Ti$ after melt spinning and nitriding.

Table 3. Results of *X*-ray analysis of the $(Nd_{0.9}Ce_{0.1})$ $Fe_{11}TiN$ alloy after melt spinning (speed = 30 m/s) and subsequent nitriding at a pressure of gaseous medium of about 40 atm and temperature of 430 °C for 40 hours.

Phase composition (Spatial group)	Volume, %	Crystal lattice parameters			Unit cell volume *V*, Å³
		a, Å *b*, Å	*c*, Å	*c/a*	
$NdFe_{11}TiN$ (139 : *I4/mmm*)	65.0(3)	8.654(9) 8.654(9)	4.922(8)	0.569	368.60(90)
α-Fe (229 : *Im-3m*)	35.0(8)	2.877(2) 2.877(2)	2.877(2)	1	23.81(30)

Table 4. Results of *X*-ray analysis of the $(Nd_{0.8}Ce_{0.2})$ $Fe_{11}TiN$ alloy after melt spinning (speed = 30 m/s) and subsequent nitriding at a pressure of gaseous medium of about 40 atm and temperature of 430 °C for 40 hours.

Phase composition (Spatial group)	Volume, %	Crystal lattice parameters			Unit cell volume *V*, Å³
		a, Å *b*, Å	*c*, Å	*c/a*	
$NdFe_{11}TiN$ (139 : *I4/mmm*)	70.0(3)	8.670(8) 8.670(8)	4.964(6)	0.573	373.10(40)
α-Fe (229 : *Im-3m*)	30.0(8)	2.869(2) 2.869(2)	2.873(2)	1	23.62(20)

Table 5. Results of *X*-ray analysis of the $(Nd_{0.7}Ce_{0.3})$ $Fe_{11}TiN$ alloy after melt spinning (speed = 30 m/s) and subsequent nitriding at a pressure of gaseous medium of about 40 atm and temperature of 430 °C for 40 hours.

Phase composition (Spatial group)	Volume, %	Crystal lattice parameters			Unit cell volume *V*, Å³
		a, Å *b*, Å	*c*, Å	*c/a*	
$NdFe_{11}TiN$ (139 : *I4/mmm*)	85.0(3)	8.689(4) 8.689(4)	4.980(7)	0.573	376.00(60)
α-Fe (229 : *Im-3m*)	15.0(8)	2.899(3) 2.899(3)	2.899(3)	1	24.38(50)

The unit cell volume of the $ThMn_{12}$ phase increases monotonically with Ce substitution, from 361.60 Å³ (x = 0) to 376.00 Å³ (x = 0.3), This 4% expansion is attributed to the larger ionic radius of Ce^{3+} compared to Nd^{3+}, combined with nitrogen interstitial occupancy. Such lattice expansion is known to strengthen the magnetocrystalline anisotropy of $ThMn_{12}$-type compounds by modifying the crystal field at rare-earth sites – a key factor foe coercivity enhancement.

3.3. Magnetic properties.

Table 6 summarizes the magnetic hysteresis properties after nitriding. Coercivity increased monotonically with Ce content, reaching 112.9 kA/m for x = 0.3. Residual magnetization also increased steadily from 16.8 to 41.5 A·m²/kg. Saturation magnetization showed a non-monotonic trend, peaking at 137.0 A·m²/kg for x = 0.2 before decreasing slightly.

Table 6. Magnetic hysteresis properties at room temperature of $(Nd_{1-x}Ce_x)Fe_{11}Ti$ alloys after melt-spinning (30 m/s) and subsequent nitriding at a pressure of gaseous medium of about 40 atm and temperature of 430 °C for 40 hours.

Sample	Coercive force ($_iH_c$, kA/m (Oe))	Residual magnetization (σ_r, A·m²/kg)	Saturation magnetization (σ_s, A·m²/kg)
$x = 0$	30.8 (387.0)	16.8	120.0
$x = 0.1$	31.8 (400.2)	20.3	112.0
$x = 0.2$	49.9 (626.5)	32.2	137.0
$x = 0.3$	112.9 (1418.0)	41.5	117.0

Two distinct compositional thresholds are observed. First, the coercivity increases only gradually up to x = 0.2 (from 30.8 to 49.9 kA/m), but then shows a dramatic jump to 112.9

kA/m at x = 0.3 – a 126% increase relative to x = 0.2. Second, the saturation magnetization exhibits a non-monotonic behavior: it peaks at x = 0.2 (137.0 A.m^2/kg) and then drops by ≈15% at x = 0.3. This suggests that moderate Ce substitution (x = 0.2) optimizes the ferromagnetic exchange, while higher Ce levels (x = 0.3) strongly enhance coercivity at the expense of saturation magnetization. The nearly four-fold increase in coercivity from x = 0 (30.8 kA/m) to x = 0.3 (112.9kA/m) correlates directly with the unit cell volume increase shown in Tables 2-5. Large unit cell creates more space for interstitial nitrogen, which in turn enhances the uniaxial anisotropy field. However, the drop in σ_s at x = 0.3 suggests that excessive Ce dilution of the Nd sublattice reduces the net magnetization, as Ce carries a lower magnetic moment (≈2.5 μ_B) compared to Nd (≈3.3 μ_B).

3.4 Effect of processing

Table 7 compares magnetic properties in as-cast (arc-melt), melt-spun, and nitrided states. Nitriding yielded the highest coercivity and residual magnetization for all compositions, with significant gains over the melt-spun state.

Table 7. Magnetic hysteresis properties at room temperature of $(Nd_{1-x}Ce_x)Fe_{11}Ti$ alloys after smelting (as cast), after melt-spinning (30 m/s) and subsequent nitriding at a pressure of gaseous medium of about 40 atm and temperature of 430 °C for 40 hours.

Sample	Coercive force ($_iH_c$, kA/m (Oe))	Residual magnetization (σ_r, A·m^2/kg)	Saturation magnetization (σ_s, A·m^2/kg)
After smelting (as cast state)			
$x = 0$	9.1 (114.3)	5.3	128.0
$x = 0.1$	9.1 (113.9)	5.4	124.0
$x = 0.2$	9.2 (115.4)	5.4	119.0
$x = 0.3$	9.3 (116.1)	5.5	116.0
After melt-spinning			
$x = 0$	15.4 (193.7)	9.3	97.3
$x = 0.1$	19.2 (240.7)	11.2	86.8
$x = 0.2$	28.3 (355.9)	15.8	97.6
$x = 0.3$	38.7 (486.4)	20.5	104.0
After nitriding			
$x = 0$	30.8 (387.0)	16.8	120.0
$x = 0.1$	31.8 (400.2)	20.3	112.0
$x = 0.2$	49.9 (626.5)	32.2	137.0
$x = 0.3$	112.9 (1418.0)	41.5	117.0

Nitriding increases coercivity by a factor of 2-3 relative to the melt-spun state across all compositions. For x = 0.3, the grain is most striking: from 38.7 kA/m (melt-spun) to 112.9 kA/m (nitride). This enhancement is not merely due to lattice expansion (which also occurs in Ce-free samples) but likely reflects a synergistic effect: Ce substitution modifies the local electronic structure, making the interstitial 2b sites more favorable for nitrogen absorption.

4. Discussion

The increase in coercivity with Ce substitution and nitriding can be attributed to a combination of lattice expansion, which enhances magnetocrystalline anisotropy, and possible grain boundary modifications that inhibit domain wall motion [1]. It is well established that interstitial nitrogen atoms occupy the 2b sites in the $ThMn_{12}$ lattice, increasing both the *a* and *c* lattice parameters [11]. This expansion modifies the crystal field at the rare-earth sites, strengthening the Nd-Fe exchange coupling and consequently, the magnetocrystalline anisotropy field [4, 12]. In this study, the unit cell volume increased monotonically from 361.60

Å^3 (x = 0) to 376.00 Å^3 after nitriding, a 4% expansion consistent with nitrogen incorporation. The nearly four-fold rise in coercivity over the same composition range (30.8 to 112.9 kA/m) directly correlates with this volume increase, supporting the primary driver of the enhanced coercivity. The observed maximum in σ_s at x = 0.2 suggests an optimal balance between ferromagnetic exchange interactions and the dilution effect of Ce, which possesses lower magnetic moments compared to Nd [19]. Moreover, from the *X*-ray diffraction studies, it was found that the alloys hardened from liquid after nitriding process. The volume of the unit cell for the main phase with $ThMn_{12}$-type increased by 5 – 7%. The observed volume effect is associated with the nitrogen atoms occupying certain positions (2b) of the crystal lattice for the intermetallic compound with $ThMn_{12}$-type structure and the formation of (Nd, Ce) $Fe_{11}TiN_{1-\delta}$ phase ($0 < \delta < 1$). The degree of dispersion of grain on the 1:12 type structure phase under practical consideration did not change compared to the hardened state. There is a clear increase on the amount of α-Fe impurity phase result to be 30 – 35 vol. % for the alloys with $x = 0.1$ and $x = 0.2$. The results of the magnetic measurement will be exhibited in the Figure 2. The figure shows the magnetic hysteresis properties of the base alloy for the third melting stage after melt-spinning (30 m/s) and subsequent nitriding with the pressure of 40 atm and the temperature of 430 °C for 40 hours. While table 6 above gives the corresponding values of the magnetic hysteresis properties of the aforementioned alloys.

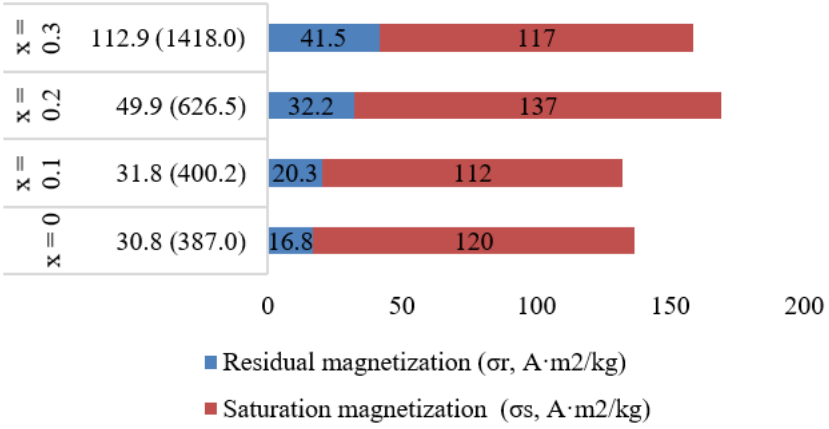

Figure 2. Magnetic hysteresis properties at room temperature of $(Nd_{1-x}Ce_x)Fe_{11}Ti$ alloys after melt-spinning (30 m/s) and subsequent nitriding at a pressure of gaseous medium of about 40 atm and temperature of 430 °C for 40 hours.

Therefore, nitriding of the quenched alloys led to a noticeable increase in the hysteresis properties compared with the previous two states investigated. For the aforementioned alloys, the coercive force and the residual magnetization result to a monotonous increase from 30.8 to 112.9 kA/m and from 9.3 to 20.5 A·m^2/kg respectively with increasing cerium ($x = 0 – 0.3$). Furthermore, the values of saturation magnetization changed non-monotonous from 120 to 117 A·m^2/kg, with a maximum value of 137 A·m^2/kg when $x = 0.2$. The increase in values for the magnetic hysteresis properties of the aforementioned samples compared to the samples produce by melt-spinning process are associated with an increase in the volume of the unit cell of the main magnetic solid phase. Furthermore, the magnetic hysteresis properties measured at room temperature and at a magnetic field strength of 20 kOe for $(Nd_{1-x}Ce_x)$ $Fe_{11}Ti$ alloys ($x = 0 – 0.3$) after various processes as shown in Figure 3.

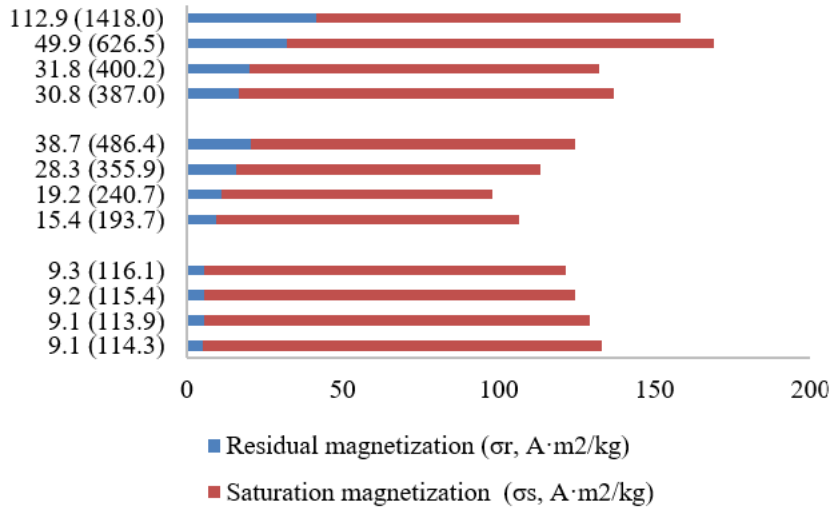

Figure 3. Magnetic hysteresis properties at room temperature of $(Nd_{1-x}Ce_x)Fe_{11}Ti$ alloys after smelting (as cast), after melt-spinning (30 m/s) and subsequent nitriding at a pressure of gaseous medium of about 40 atm and temperature of 430 °C for 40 hours.

The higher α-Fe fraction for x = 0.1–0.2 may contribute to the enhanced σ_s by providing soft magnetic coupling, although excessive α-Fe could deteriorate coercivity. The interplay between phase composition and nitrogen-induced anisotropy is therefore critical for optimizing magnetic performance. The observed maximum in σ_s at x = 0.2 (137.0 A.m^2/kg) coincides with the highest α-Fe volume fraction (30-35%, Tables 3-4). This is consistent with a soft magnetic coupling mechanism: finely dispersed α-Fe grains exchange couple with the hard $ThMn_{12}$ matrix, enhancing the overall remanence and saturation magnetization via the exchange spring effect. A similar phenomenon has been reported in rapidly solidified Nd-Fe-B based alloys and in other $ThMn_{12}$ systems [8]. At x = 0.3, the α-Fe fraction drops to 15% and σ_s correspondingly decreases to 117.0 A.m^2/kg, suggesting that an optimal α-Fe content exist for maximizing saturation under the present processing conditions. Conversely, the monotonic rise in coercivity with x (despite decreasing α-Fe fraction) indicates that the intrinsic anisotropy enhancement from Ce substitution and nitriding dominates over any soft magnetic dilution effects. Figure 4, expressed how the coercivity and remnance increased monotonically, with a sharp rise at x = 0.3. Saturation magnetization peaks at x = 0.2 and declines at x = 0.3, indicating an optimal balance between Ce-induced anisotropy enhancement and magnetic moment dilution.

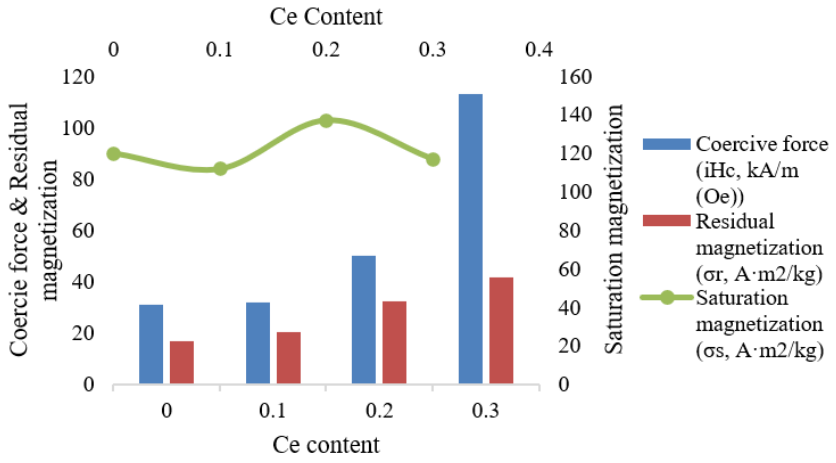

Figure 4. Magnetic properties of nitride $(Nd_{1-x}Ce_x)Fe_{11}Ti$ as a function of Ce content.

A notable observation from the structural analysis is that the volume expansion of the $ThMn_{12}$ unit cell upon nitriding is largest for the Ce-containing samples (from 361.60 Å^3 at x = 0 to 376.00 Å^3 at x = 0.3). This is consistent with earlier reports by Fang et al. [11], who found that the $CeFe_{11}Ti$ system exhibits isotropic lattice expansion upon nitrogenation, with the largest volume increase among all $RFe_{11}Ti$ compounds (R = Ce, Pr, Nd). They attributed this behavior to dramatic change in the Ce-4f electron state upon nitrogen uptake, which in turn affects the local crystal field and, consequently, the magnetocrystalline anisotropy. The present results support this interpretation: the most Ce rich sample (x = 0.3) shows both the largest unit cell and the highest coercivity, suggesting that the Ce specific electronic effect contributes synergistically to the anisotropy enhancement.

The present results are in good agreement with earlier work by Zheleznyi et al. [21], who found that the optimal magnetic properties in nitride $(Nd_{1-x}Ce_x)Fe_{11}Ti$ alloys are obtained at x = 0.2 and 0.3. However, the coercivity values reported here (112.9 kA/m at x = 0.3) are substantially higher than those obtained in the earlier study under similar processing conditions. The most likely explanation for this difference is the longer nitriding time used in the present work (40 h vs. 20 h), which may have allowed more complete nitrogen diffusion into the $ThMn_{12}$ lattice, particularly for the Ce-rich composition. The magnetic performance achieved in the present study can be benchmarked against recent DFT predictions.

The maximum energy product $(BH)_{max}$ of 365 kJ/m^3 and Curie temperature of 593 K were calculated for (Nd,Ce)$Fe_{11}Ti$ magnets, with a theoretical magnetic hardness factor κ = 1.20, qualifying them as good candidates for rare-earth-lean permanent magnets [9]. While direct experimental determination of $(BH)_{max}$ was not performed here, the measured saturation magnetization (137.0 A·m^2/kg) and coercivity (112.9 kA/m) are consistent with these theoretical predictions. This agreement validates the computational approach and suggests that further optimization of grain structure and nitrogen content could bring experimental $(BH)_{max}$ closer to the theoretical limit.

The anisotropy enhancement observed here is consistent with studies on other $ThMn_{12}$ systems. Wang et al. [8] reported that nitrogenation of $NdFe_{10}V_2$ compounds transforms the magnetocrystalline anisotropy from weak uniaxial to strong uniaxial, with a corresponding increase in coercivity. Similarly, Katter et al. [6] demonstrated that interstitial nitrogen significantly raises both the Curie temperature and anisotropy field in Mo-stabilised compounds. The present work extends these findings to Ce-substituted $NdFe_{11}Ti$, showing that partial replacement of Nd by Ce does not diminish the beneficial effect of nitriding; on contrary, for x = 0.3, the coercivity enhancement is even more pronounced than in the Ce-free reference sample. This suggests that Ce substitution and nitriding act synergistically, rather than antagonistically, in modifying the anisotropy.

The maximum coercivity achieved here (112.9 kA/m at x = 0.3) is comparable to values reported for other $ThMn_{12}$-based nitrides. Fang et al. [11] obtained coercivities in the range of 100 – 150 kA/m for nitrided Nd-Fe-Mo melt-spun ribbons, while Zheleznyi et al. [21] reported values of approximately 80 kA/m for similar Ce-substituted compositions. The present improvement over the latter can be attributed to the extended nitriding time (40 h vs. 20 h) and an optimized melt-spinning parameters (wheel speed 30 m/s), which produced finer and more uniform grain structure. Nevertheless, the coercivity remains significantly lower than that of commercial $Nd_2Fe_{14}B$ magnets (typically > 1000 kA/m), indicating that further microstructural

refinement such as grain boundary engineering or reduction of α-Fe content is still required for practical applications.

5. Conclusion

This study demonstrates that Ce substitution and nitriding of $(Nd_{1-x}Ce_x)Fe_{11}Ti$ alloys significantly enhance coercivity and residual magnetization compared to as-cast and melt-spun states. This work provides the first systematic demonstration that Ce substitution up to x = 0.3, combined with high-pressure nitriding, yields a near-four-fold increase in coercivity compared to Ce free nitride alloys, while maintaining competitive saturation magnetization at x = 0.2. these findings are novel because they reveal a synergistic effect between Ce-induced lattice expansion and nitrogen interstitial occupancy – an interaction not previously quantified for this alloys system. By replacing 20 – 30% of Nd with more abundant and less expensive Ce, the present alloys reduce reliance on critical rare-earth elements without sacrificing permanent magnet performance. The optimal composition for balancing high coercivity and high saturation magnetization is x = 0.2, which achieved $\sigma_s = 137.0$ A·m²/kg. These findings support the potential of partially Ce-substituted $NdFe_{11}TiN$ alloys as cost-effective, high-performance permanent magnet materials. Several avenues for future research emerge from these results. First, the long-term thermal stability of (Nd, Ce)$Fe_{11}TiN$ magnets should be evaluated, as interstitial nitrogen can be lost at elevated temperatures, degrading coercivity. Accelerated aging test under oxidative and humid conditions are recommended. Second, alternative dopants such as Sm, Pr and La could be explored in combination with Ce to further tune anisotropy and saturation magnetization. Third, optimization of melt-spinning and nitriding parameters could reduce the α-Fe volume fraction (currently 30 – 35% for x = 0.1 – 0.2). Fourth, microstructural engineering (e.g., grain boundary diffusion or intergranular phases) may enhance coercivity further. Finally, direct measurement of the maximum energy produc $(BH)_{max}$ for x = 0.2 composition would allow quantitative benchmarking against commercial $Nd_2Fe_{14}B$ magnets.

Availability of data and materials

All data used was presented on the manuscript, but if more required, the data will be available on request.

Competing interests

There is no any competing interest with the authors.

Funding

There is no funding received.

Authors' contributions

The manuscript draft, written and research conducted by the author "Jamal Shehu" under the supervision of "Prof. Igor V. Shchtenin" and "Prof. Alexy O. Rodin".

References

[1] Coey, J.M.D. (2011). Magnetism and Magnetic Materials; Cambridge University Press: Cambridge, United Kingdom.

[2] Skomski, R.; Coey, J.M.D. (2016). Permanent Magnetism; CRC Press: Boca Raton, FL, USA.
[3] Hirosawa, S.; Matsuura, Y.; Yamamoto, H.; Fujimura, S.; Sagawa, M.; Osamura, K. (1986). Magnetization and magnetic anisotropy of $R_2Fe_{14}B$ measured on single crystals. *Journal of Applied Physics*, *59*(3), 873–879. https://doi.org/10.1063/1.336611.
[4] Chakraborty, M.; Jensen, G.; Ingram, D.C.; Stinaff, E.; Jadwisienczak, W.M. (2025). Magnetic Properties of Nitrogen-Doped Graphene Induced by Dopant Configurations. *Nanomaterials*, *15*, 1694. https://doi.org/10.3390/nano15221694.
[5] Gutfleisch, O.; Xu, B.; Dirba, I.; et al. (2018). $ThMn_{12}$-type alloys for permanent magnets. *Engineering*, *4*(4), 436–441. https://doi.org/10.1016/j.eng.2018.12.011.
[6] G.C. Hadjipanayis, A.M. Gabay, A.M. Schönhöbel, A. Martín-Cid, J.M. Barandiaran, D. Niarchos. (2020). ThMn12-Type Alloys for Permanent Magnets. *Engineering*, *6*(2), 140−146 https://doi.org/10.1016/j.eng.2018.12.011.
[7] Harashima, Y.; Terakura, K.; Kino, H.; Ishibashi, S.; Miyake, T. (2015). Nitrogen as the best interstitial dopant among X = B, C, N, O, F for strong permanent magnet $NdFe_{11}TiX$: First-principles study. *arXiv Preprint*. Available online: https://arxiv.org/abs/1507.03777.
[8] Camacho-Peralta, M.A.; Betancourt, I.; Elizalde-Galindo, J.T. (2026). Phase Transformation and Magnetic Properties of Rapidly Solidified Mn-Al Alloys. *Condensed Matter*, *11*, 12. https://doi.org/10.3390/condmat11020012.
[9] Saito, T.; Wang, W.; Kamagata, Y. (2005). Structures and magnetic properties of Nd–Fe–Ti alloys produced by melt-spinning technique. Journal of Alloys and Compounds. *Journal of Alloys and Compounds*, *417*(1–2), 109–114. https://doi.org/10.1016/j.jallcom.2005.03.091.
[10] Ying, W.; Yang, Z.; Liu, X.; Yao, Q.; Wang, J. (2025). Effects of Lanthanum Element and Heat Treatment on Phase Formation and Magnetic Properties of $SmFe_{10}V_2$ Melt-Spun Ribbons. *Materials*, *18*, 2322. https://doi.org/10.3390/ma18102322.
[11] Zeng, W.; He, X.; Luan, B.; Ren, S.; Liao, X.; Zhou, Q. (2026). Phase Structure and Magnetic Properties of Nanocrystalline $ThMn_{12}$-Type $(Nd_{1-x}Sm_x)_{1.2}Fe_{10.5}Mo_{1.5}$ Alloys. *Materials*, *19*, 930. https://doi.org/10.3390/ma19050930.
[12] Fukazawa, T.; Akai, H.; Harashima, Y.; Miyake, T. (2016). First-principles study of intersite magnetic couplings in $NdFe_{12}$ and $NdFe_{12}X$ (X = B, C, N, O, F). *arXiv Preprint*. Available online: https://arxiv.org/abs/1612.04478.
[13] Körner, W.; Krugel, G.; Elsässer, C. (2016). Theoretical screening of intermetallic $ThMn_{12}$-type phases for low-RE hard magnets. *Scientific Reports*, *6*, 24686. https://doi.org/10.1038/srep24686.
[14] Miyake, T.; Terakura, K.; Harashima, Y.; Kino, H.; Ishibashi, S.. (2014). First-principles study of magnetocrystalline anisotropy and magnetization in $NdFe_{12}$, $NdFe_{11}Ti$ and $NdFe_{11}TiN$. *Journal of the Physical Society of Japan*, *83*, 043702. https://doi.org/10.7566/JPSJ.83.043702.
[15] Miyake T, Harashima Y, Fukazawa T, Akai H. (2021). Understanding and optimization of hard magnetic compounds from first principles. *Science and Technology of Advanced Materials*, *22*, 735–771. https://doi.org/10.1080/14686996.
[16] Xu, C.; Wen, L.; Pan, A.; Zhao, L.; Liu, Y.; Liao, X.; Pan, Y.; Zhang, X. (2024). First-Principles Study of Ti-Doping Effects on Hard Magnetic Properties of RFe11Ti Magnets. *Crystals*, *14*, 507. https://doi.org/10.3390/cryst14060507.
[17] Shehu, J.; Shetinin, I. (2023). Effect of Ce doping on the magnetic properties of $NdFe_{11}Ti$ alloys. *SSRN Preprint*. https://doi.org/10.2139/ssrn.4653860.
[18] Shehu, J.; Shchetenin, I.V. (2023). Magnetic properties of $(Nd_{1-x}Ce_x)Fe_{11}Ti$ alloys produced by melt-spinning process. *Materials Today Communications*, *37*, 107450. https://doi.org/10.1016/j.mtcomm.2023.107450.
[19] Wang, K.; Yu, J.; Chi, C.; Zhang, G. (2022). Magnetic Properties in Mn-Doped δ-MoN: A Systematic Density Functional Theory Study. *Nanomaterials*, *12*, 747. https://doi.org/10.3390/nano12050747.

[20] Pathak, A.K.; Khan, M.; Paudyal, D.; Gschneidner, K.A.; Pecharsky, V.K. (2015). Cerium: An unlikely replacement of dysprosium in high-performance Nd–Fe–B permanent magnets. *Advanced Materials*, *27*(16), 2663–2670. https://doi.org/10.1002/adma.201404892.

[21] Zheleznyi, M.V.; Shchetinin, I.V.; Gorshenkov, M.V.; Bazlov, A.I.; Zanaeva, E.N.; Hudina, E.V.; Savchenko, A.G. (2018). Structure and magnetic hysteresis properties of rapidly quenched $Nd_{1-x}Ce_x(Fe_{0.75}Co_{0.25})_{11}Ti$ (x = 0–0.3) based alloys after annealing. *Journal of Physics: Conference Series*, *1134*, 012074. https://doi.org/10.1088/1742-6596/1134/1/012074.

© 2026 by the authors. This article is an open access article distributed under the terms and conditions of the Creative Commons Attribution (CC BY) license (http://creativecommons.org/licenses/by/4.0/).